Indian Journal of Pure & Applied Physics
Vol. 57, January 2019, pp. 14-22

Effect of calcination on the structural, optical and magnetic properties of $BaWO_4$ nanoparticles synthesized by chemical precipitation

Seenamol K Stephen[a], Aloysius Sabu N[b], Priyanka K P[b] & Thomas Varghese[b]*

[a]T M Jacob Memorial Government College, Manimalakkunnu, Koothattukulam 686 662, India
[b]Nanoscience Research Centre (NSRC), Nirmala College, Muvattupuzha 686 661, India

Received 26 June 2017; accepted 23 August 2018

$BaWO_4$ nanoparticles have been synthesized by chemical precipitation method using barium nitrate and sodium tungstate. Thermogravimetric analysis has been done to determine the thermal behaviour of the sample. The synthesized nanoparticles have been calcined at 400, 550 and 700 °C for 3 h to get well defined crystalline nanoparticles. As synthesized samples have been characterized by X-ray diffraction, Fourier transform infrared spectroscopy, Raman spectroscopy, scanning electron microscopy, transmission electron microscopy, UV-Visible absorption and photoluminescence spectroscopy. Magnetic properties of the samples have been studied by vibrating sample magnetometer measurements. The effect of calcination temperature on the structural, optical and magnetic properties of $BaWO_4$ has also been investigated.

Keywords: $BaWO_4$ nanoparticles, Structural properties, Optical properties, Magnetic properties

1 Introduction

Tungstate nanoparticles have received wide spread attention due to its novel structural, electrical, optical and magnetic properties. They have found many applications in various fields, such as electrical and humidity sensors[1,2], oscilloscopes[3], light emitting diodes (LEDs)[4-6], gas sensors[4]. Among tungstates, barium tungstate with scheelite structure is important because of its blue luminescence. It has found many applications in the field of fluorescent lamps, optoelectronic devices and display systems[5]. Barium tungstate has been prepared by different methods, such as solid state reaction[6], microwave irradiation method[7], template free precipitation technique[8], co-precipitation method[9], sucrose templated method[10], modified combustion technique[11], sucrose solution evaporation method[12], electrochemical synthesis[13], catanionic reverse micelles involvingpolymers[14], sonochemical method[15], microwave hydrothermal synthesis[16], polymeric precursor method[17]and precipitation method[18].

Here we report synthesis and characterization of $BaWO_4$ nanoparticles by chemical precipitation method without using any surfactant. As synthesized nanoparticles are thermally characterized by thermogravimetric and differential thermogravimetric analysis (TGA/DTG); structurally characterized by X-ray diffraction (XRD), scanning electron microscopy (SEM), transmission electron microscopy (TEM), Fourier transform infrared spectroscopy (FTIR) and Raman spectroscopy; optically characterized by UV-Visible absorption and photoluminescence (PL) spectroscopy. The magnetic properties of the $BaWO_4$ nanoparticles are explored using vibrating sample magnetometer (VSM). The effect of calcination temperature on the structural, optical and magnetic properties of the synthesized nanoparticles is also investigated. The results obtained from the systematic investigations revealed that $BaWO_4$ nanoparticles have potential in varied applications, such as visible light photocatalysis, and optoelectronic devices.

*Corresponding author (E-mail:nanoncm@gmail.com)

2 Experimental Details

Barium nitrate ($Ba(NO_3)_2$) (99%, Merck) and sodium tungstate ($NaWO_4.2H_2O$) (98%, Merck) were used without further purification for the synthesis of $BaWO_4$.

2.1 Preparation of the sample

0.1 M solution each of barium nitrate and sodium tungstate was prepared by dissolving the desired quantity of them in distilled water. Sodium tungstate solution was added to barium nitrate solution drop by drop, and the mixture solution was then stirred well for about 30 min using a magnetic stirrer at room temperature. The white precipitate formed was

washed well with distilled water several times to remove the unreacted reagents and sodium nitrate formed. The product obtained was dried in a hot air oven at 80 °C for about 8 h. The dried particles were calcined at 400, 550, and 700 °C for 3 h in a muffle furnace. $BaWO_4$ samples calcined at 400, 550 and 700 °C are denoted as S_1, S_2 and S_3, respectively.

2.2 Characterization technique

Thermogravimetric analysis of the precursor was carried out from 40 to 730 °C at 20 °C/min using Perkins Elmer, Diamond Instrument STA 6000. The structural characterization of the samples were done by X-ray powder diffraction using Brucker AXS D8 advance X-ray diffractometer (λ=1.5406 Å, step size=0.02° and step time 29.1s) with CuKα radiation in 2θ range from 5 to 80°). The surface morphology of the samples was analyzed using scanning electron microscope JOEL model JEK-6390 LV. TEM images were recorded on Joel JEM 2100 at an accelerating voltage of 200 kV. FTIR spectra were recorded using Thermo Nicolet, Avatar 370 in a spectral range 600 to 4000 cm^{-1}. Raman spectra of the samples were taken using confocal Raman microscope with AFM (excitation laser of wavelength 633 nm). Diffuse reflectance spectra of the samples were taken using Schimadzu 2600 UV-Visible spectrophotometer in a wavelength range of 200 to 800 nm. The photoluminescence spectra of the samples were taken using Horiba Fluorolog 3 with Xe-lamp as excitation. The hysteresis loop of the samples were drawn at room temperature by taking measurements with vibrating sample magnetometer (Lakeshore VSM 7410) at room temperature in an applied magnetic field sweeping between ± 15000 Oe.

3 Results and Discussion

3.1 TG/DTG analysis

Figure 1 shows the thermal decomposition result of the precursor from the ambient temperature to 700 °C using both the thermogravimetric and differential thermogravimetric curves. Only 3% weight loss occurs in the temperature range from 100 to 700 °C. This is due to the loss of surface water on the particles, and combustion of minor impurities present in the sample. The exothermic curve of DTG confirms the combustion of the minor impurities in the sample. DTG curve remains almost constant, and only a small dip is observed at 602 °C due to the faster combustion of the impurity. The thermal analysis shows that the

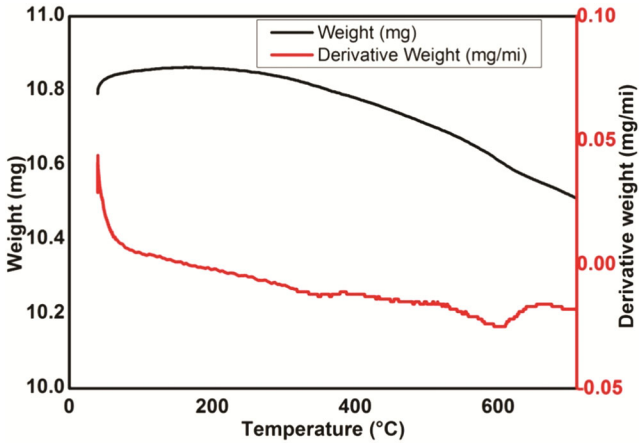

Fig. 1 – TG/DTG curves of $BaWO_4$ nanoparticles.

$BaWO_4$ nanoparticles are thermally stable above 300 °C. Hence, temperatures 400, 550 and 700 °C have been selected for calcination treatment.

3.2 XRD analysis

The phase purity, crystallinity and structure of powder samples were examined using XRD. Figure 2 shows XRD patterns of the $BaWO_4$ samples calcined at different temperatures. The well-defined diffraction peaks are obtained for the planes (101), (112), (004), (200), (211), (204), (220), (116), (132), (224), (400), (208), (316), (413), (404), (240), (228) and (110), which correspond to tetrahedral crystal structure with a space group $I4_1/a$ for $BaWO_4$ (JCPDS file No. 72-0746 of $BaWO_4$). No impurity peaks were detected in the spectra. Therefore, the present chemical precipitation method is a successful method for the synthesis of $BaWO_4$ nanoparticles. Lattice parameters of the samples were calculated using plane spacing equation for tetragonal structure[19]. Lattice parameters obtained from XRD data are presented in Table 1. The intensity of the diffraction peaks observed is minimum for S_2, while the lattice parameters and the spacing are found to be maximum for S_2.

Figure 2 and Table 1 show that the full width at half maximum (FWHM) of the diffraction peaks of the samples gradually decreases with calcination temperature. This is because at higher calcination temperature, the formed crystallites are large in size, which can be attributed to the thermally promoted crystallite growth[20]. The crystallite sizes of the samples were calculated from the line broadening of the diffraction peaks using Scherrer'sformula[21,22].

$$D = k\lambda/\beta\cos\theta, \quad \ldots (1)$$

Table1 – Geometric parameters of $BaWO_4$ samples.

Sample	$a = b$ (Å)	c (Å)	Unit cell volume (Å^3)	Crystallite size (nm)	Micro strain
S_1	5.5894	12.658	395.45	28.578	0.00146
S_2	5.6246	12.757	403.58	32.167	0.00101
S_3	5.6160	12.730	401.52	37.206	0.00076

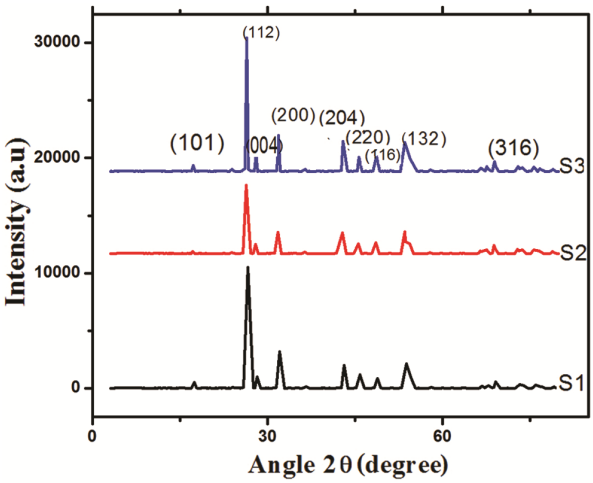

Fig. 2 – XRD patterns of $BaWO_4$ samples.

where λ is the wavelength of light used, β the full width half maximum of the sample, θ the angle of diffraction and k is a constant equal to 0.9. The crystallite sizes estimated for samples S_1, S_2 and S_3 are 28.58, 32.17 and 37.20 nm, respectively. The micro-strain or micro-diffraction values obtained from Williamson-Hall analysis[22] are 0.00146, 0.00101 and 0.000767, respectively, for S_1, S_2, and S_3.

The micro-strain of the samples is due to the presence of O vacancies, structural imperfections and surface defects, which in turn results XRD line broadening. As the calcination temperature increases the structural defects probably reduced, and hence the micro diffraction decreases. In short, calcination temperature influences the geometrical parameters of $BaWO_4$ nanoparticles.

3.3 Energy dispersive X-ray spectroscopy (EDS)

EDS is an analytical technique for the elemental analysis or chemical characterization of the as prepared sample. The EDS spectrum of the $BaWO_4$ nanoparticles calcined at 400 °C is shown in Fig. 3. It clearly shows the co-existence of barium, tungsten and oxygen in the sample in stoichiometric ratios. Absence of other elemental peaks in the spectrum exhibits the purity of the prepared $BaWO_4$ nanoparticles.The elemental composition of $BaWO_4$ sample is presented in Table 2.

Table 2 – Elemental composition of $BaWO_4$ sample.

Element	Mass %	Atom %
W L	51.03	16.53
Ba L	30.05	13.03
O K	18.92	70.43
Total	100	100

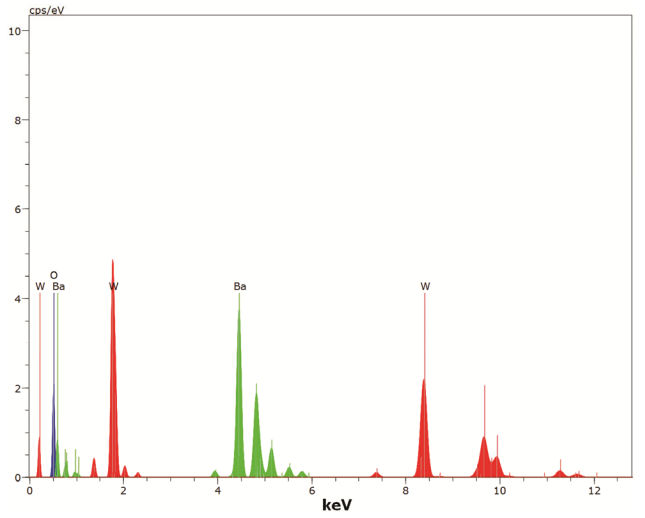

Fig. 3 – Chemical composition of $BaWO_4$ sample.

3.4 SEM analysis

For taking the SEM micrograph, a small amount of $BaWO_4$ powder is dispersed in ethanol. A drop of the suspension was placed on the carbon tape attached on the stub. It is then kept for about 5 to 10 min under infrared lamp for drying before scanning for micrographs. Figure 4 shows the SEM images of $BaWO_4$ nanoparticles calcined at 400 (S_1), 550 (S_2) and 700 °C (S_3).

The SEM images represent the surface morphology of the samples. It can be seen from Fig. 4 that the morphology of the samples changes with calcination temperature. The figure shows that sample S_1 is granular like, S_2 is popcorn shaped and S_3 has flower like morphology. As the temperature increases agglomeration of the particles takes place. The crystallinity of the sample is also increased as calcinations temperature increased. It can be seen that surface of the particles is roughly porous. As the calcination temperature increases the surface

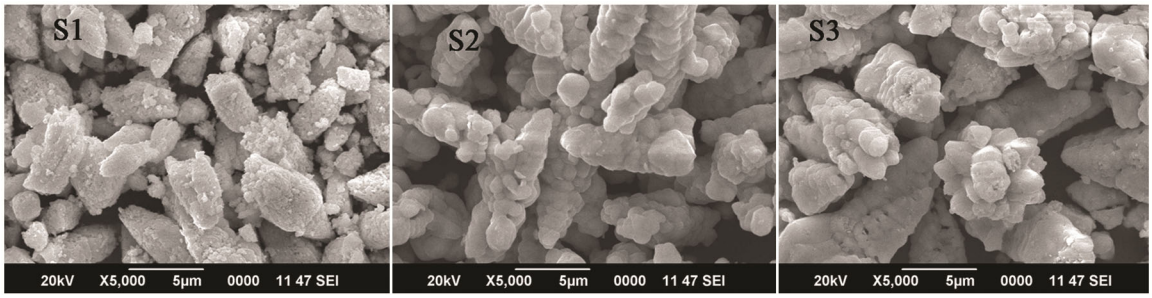

Fig. 4 – SEM images of $BaWO_4$ samples.

becomes smooth. The porosity of nanomaterials greatly influences the quality and utility of solid phase chemicals including agrochemicals, additives and pharmaceutical ingredients. It plays major roles in the purification, processing and blending of chemical products. In short, porous materials can help to design successful product and process development[23].

3.5 TEM analysis

TEM images of the samples have been recorded for analyzing the morphology and size of the synthesized products. For recording the TEM, $BaWO_4$ nanoparticle samples were initially dispersed in ethanol. A drop of the suspension was placed on a carbon coated copper grid and analyzed using a JEOL, JEM 2100 operated at 200 kV. Figure 5 shows the TEM bright field images and selected area electron diffraction (SAED) patterns of the samples calcined at different temperatures. It is found that the particles are almost spherical in shape, and agglomerated. Strong bright spots in the SAED pattern represent the crystalline nature of the sample. These bright spots are produced by the electrons reflected and diffracted from the different crystallographic planes of the unit cells of $BaWO_4$.

3.6 FTIR analysis

The FTIR spectra of the $BaWO_4$ samples S_1, S_2 and S_3 were recorded in the transmittance mode and are shown in Fig. 6. The spectra have several significant peaks recorded in the range of 4000 to 400 cm^{-1}. IR active modes of $BaWO_4$ samples are given in Table 3.

Since $BaWO_4$ has tetrahedral symmetry, F2(ν3,ν4) modes are infrared active only. The absorption peak at 403 cm^{-1} can be assigned to F2(ν4) vibration, which represents the bending vibration W-O[5]. The anti-symmetric stretching vibration F2(ν3) originating from the W-O in the WO_4^{2-} tetrahedron corresponds to the broad intense peak centered[13] at 820 cm^{-1}. The broad absorption band centered at

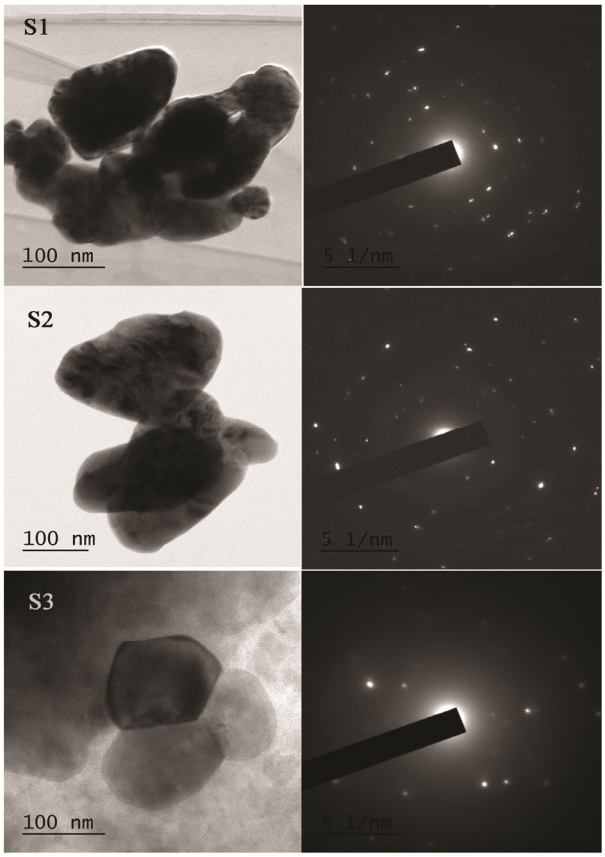

Fig. 5 – TEM images of $BaWO_4$ samples.

3450 cm^{-1} and the sharp peak centered at 1430 cm^{-1} are assigned to O-H stretching vibrations and the O-H bending vibrations[24], respectively. The band centered at 1630 cm^{-1} is attributable to H-O-H bending vibration mode[25]. In brief, the direct precipitation method used in the present work is suitable synthesis route to obtain the tetrahedral $BaWO_4$ nanoparticles with the characteristics bonds.

3.7 Raman studies

Raman spectra of the samples were taken to verify the rotational, vibrational and other low

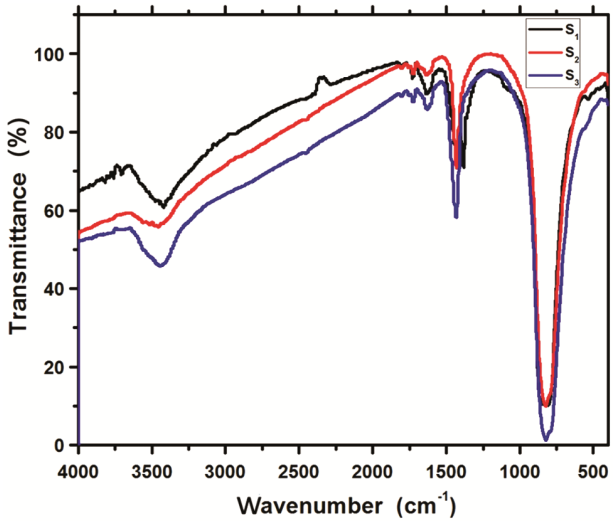

Fig. 6 – FTIR spectra of the $BaWO_4$ samples.

Table 3 – IR active modes of $BaWO_4$ samples.

Peaks observed (cm^{-1})		
S_1	S_2	S_3
3426	3456	3456
1633	1632	1630
1433	1433	1433
827	827	819
403	403	403

frequency modes of the system. From group theory the vibrational representations at the Γ point scale for scheelite $BaWO_4$ is given by:

$$\Gamma = (3Ag+3Bu) + (5Bg+5Au) + (5Eg+5Eu), \quad \ldots (2)$$

Where A and B modes are degenerate, and E modes are non-degenerate. The sub-index *g* and *u* stand for even and odd parity. One Au and one Eu correspond to the zero frequency acoustic modes and the rest are optic modes. In $BaWO_4$, the first member of pairs is Raman active. The second member of pairs is infrared active except for the Ba silent modes that are not infrared active. There will be 13 Raman active modes for $BaWO_4$,

$$\Gamma = 3Ag + 5Bg + 5Eu. \quad \ldots (3)$$

The Raman spectra of scheelite $BaWO_4$ contain internal and external mode of vibration. In the internal mode of vibration, the centre of mass does not move and the vibrations are within the $[WO_4]2-$ molecule. The external mode of vibration corresponds to the motion of Ba+ cation and the rigid molecular unit[12,13]. Figure 7 depicts Raman spectra of the samples S_1, S_2 and S_3.

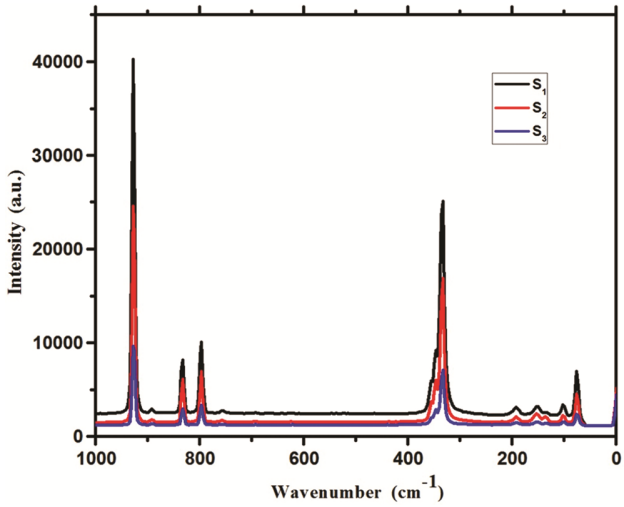

Fig. 7 – Raman spectra of $BaWO_4$ samples.

Table 4 compares Raman active modes of $BaWO_4$ samples with literature values. Here ν_1, ν_2, ν_3 and ν_4 represent the internal mode of vibrations, *R* and *T* represent the rotational and translational mode of vibrations. It is found that maximum shift is observed for Raman vibration modes for sample S_2, which has the highest unit cell volume. It can be seen that the experimental values observed are in agreement with the reported values. Two additional peaks are also obtained at 754 cm^{-1} and 891 cm^{-1} for samples S_1 and S_2. This may be due to impurities present in the sample. But the XRD, EDAX and FTIR results excluded the presence of impurities. Hence we can conclude that the absorption peak at 891 cm^{-1} is due to the symmetric stretching vibration of the short W-O bond in the WO_2 group and the absorption at 754 cm^{-1} is due to the surface disordered layers or due to the strain present in the prepared sample[26]. The intensity and FWHM of the Raman modes decrease as the calcinations temperature increases, which is due to the change in surface morphology of the samples. As can be seen from the SEM photographs, the surface becomes smooth as calcinations temperature increases. Hence, the absorption as well as emission decreases or the particles become more crystalline with calcination.

3.8 UV-Visible absorption studies

UV-Visible absorption spectra of the samples were taken to analyze their optical absorption properties. Figure 8 shows the optical absorption spectra of calcined samples of $BaWO_4$. The optical absorption is observed only in the ultraviolet region of the spectra. The absorption peak corresponding to the

Table 4 – Comparison of Raman active modes of $BaWO_4$ samples with literature values.

Peak/mode	Value of ω in cm^{-1}						
	Theo.[1]	Present values				Literature values	
		S_1	S_2	S_3		Lit.[12] Lit.[11] Lit.[25]	
T(Bg)	55	-	55	-	-	63	62
T(Eg)	81	75	81	75	-	75	74
T(Eg)	110	101.7	110	101	-	102	104
T(Bg)	145	150.6	145	151.9	-	133	132
R(Ag)	149	-	149	-		150	150
R(Eg)	209	191	209	191	272	191	191
ν2(Ag)	328	332	328	332	330	331	-
ν2(Bg)	329	333	329	333	-	333	332
ν4((Bg)	339	345.6	339	346	-	345	345
ν4(Eg)	348	354.9	348	354.5	-	355	353
ν3(Eg)	797	796	797	796	797	794	796
ν3(Bg)	823	831.6	823	831.6	829	831	830
ν1(Ag)	928	928	928	927.6	924	925	925

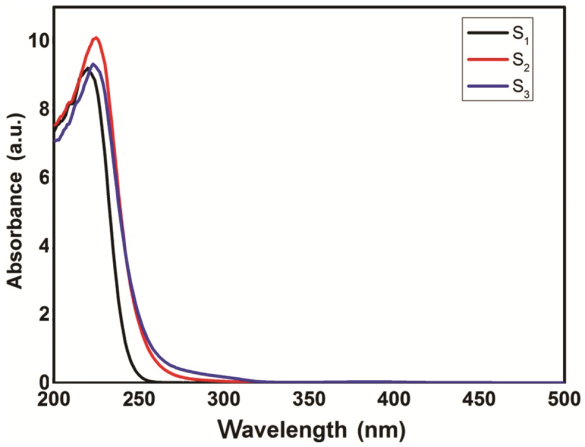

Fig. 8 – UV-Visible absorption spectra of $BaWO_4$ samples.

samples S_1, S_2, and S_3 are at 220, 224 and 223 nm, respectively. The small red shift with increase in calcinations temperature is due to increase in particle size caused by the calcination.

Tauc plot of the $BaWO_4$ samples calcined at different temperatures is depicted in Fig. 9. Tauc relationship was used to calculate the bandgap of the nanoparticles. The bandgap values estimated for S_1, S_2 and S_3 are 5.25, 5.14 and 5.13 eV, respectively. These values are slightly greater than the reported value 4.6 eV[13]. The UV-Visible absorption studies show that optical bandgap decreases with increase in calcination temperature due to crystal growth caused by calcination.

3.9 Photoluminescence studies

The PL spectra of the $BaWO_4$ samples with an excitation wavelength of 388 nm are shown in Fig. 10. One intense peak is observed at 428 nm and two weak peaks at 531 and 640 nm. The blue emission (428 nm) is due to the charge transfer transitions between the O2p orbits and the empty d orbits of the central W^{6+} ions in $[WO_4]^{2-}$ tetrahedron[13]. The other two peaks are due to structural distortions in the crystal lattice. Here the emission peaks are sharp, since calcination reduces the defects in the crystal structure and the crystals become highly ordered. The PL emission is found to be in visible regime for all the samples, and the intensity of emission is found maximum for the sample S_3. Thus, PL emission can also be tuned by changing calcination temperature. In short, the PL studies suggested that the synthesized $BaWO_4$ nanoparticle samples are useful for photocatalytic applications.

3.9.1 CIE chromaticity

The CIE serves as a standard reference against which many other colour spaces are defined. The chromaticity of a colour is designated by projection co-ordinates *x* and *y*. The CIE chromaticity co-ordinates under 388 nm excitation of the $BaWO_4$ samples S_1, S_2 and S_3 are (0.22364, 0.251694), (0.242682, 0.29394) and /0.243769, 0.296648/ respectively. Figure 11 shows the CIE chromaticity diagram for the samples S_1, S_2 and S_3. All the three samples show blue-green emission with slight changes for the chromaticity co-ordinates. The CIE results show that $BaWO_4$ phosphors can be used in fluorescent lamps, electronic display and other optoelectronic applications.

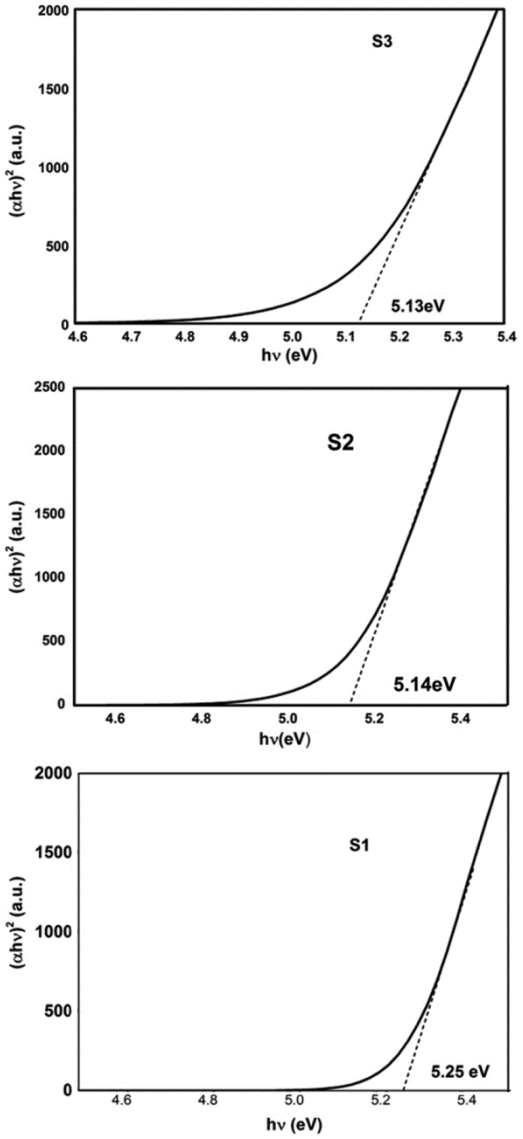

Fig. 9 – Tauc plots of the $BaWO_4$ samples.

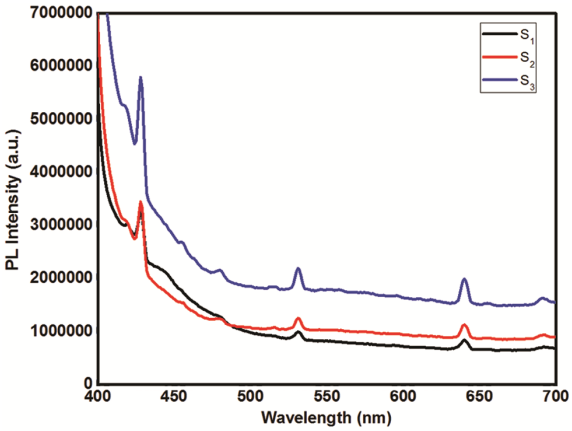

Fig. 10 – PL spectra of $BaWO_4$ samples.

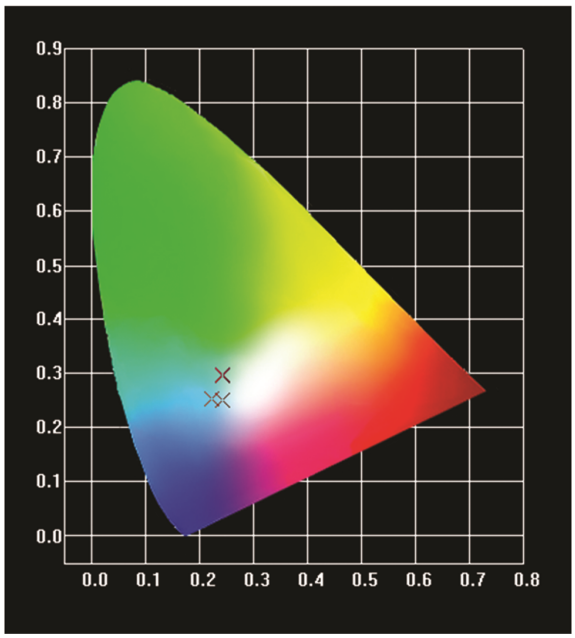

Fig. 11 – The CIE Chromaticity diagram for $BaWO_4$ samples.

3.10 Magnetic properties

The magnetic properties of the $BaWO_4$ nanoparticle samples were studied using VSM measurements. The hysteresis curves for the samples S_1, S_2 and S_3 are shown in Fig. 12. It can be seen that the samples show ferromagnetic behavior. The saturation magnetization values are very low because of the absence of unpaired electrons in barium, and it agrees with the literature values[18]. The variation of coercivity, saturation magnetization, retentivity and squareness ratio *R* of the samples are presented in the Table 5. Fig.12 and Table 5 confirm that saturation magnetization and coercivity of the $BaWO_4$ samples varies with calcinations temperature.

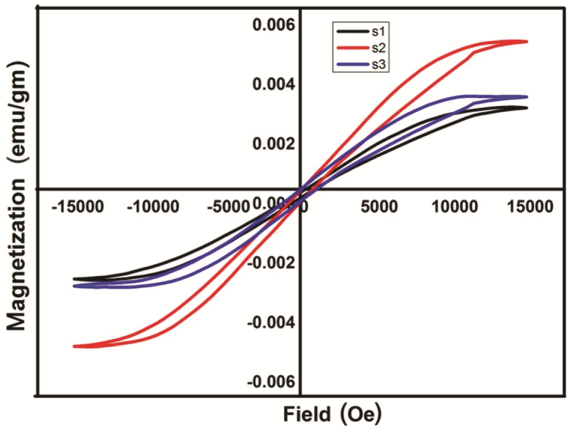

Fig. 12 – Magnetic hysteresis curves for $BaWO_4$ samples.

Table 5 – Comparison of magnetic properties of the samples.

Sample	Saturation magnetization (Ms)	Coercivity (Oe)	Retentivity (Mr)	Squareness ratio *R*=Mr/Ms
S_1	3.229 ×10-3 emu/g	302.44	57.69×10^{-6}	0.0178
S_2	5.783 × 10-3 emu/g	361.63	455.05×10^{-6}	0.0787
S_3	3.4965 ×10-3 emu/g	407.04	388.2×10^{-6}	0.111

The saturation magnetization is maximum for the sample calcined at 550 °C (S_2), which has the highest value of lattice parameters. It is interesting that the change in saturation magnetization and retentivity are in accordance with the change in lattice parameters of the sample with calcinations temperature. The saturation magnetization is found to be maximum for the sample (S_2) with maximum unit cell volume[27]. Since the squareness ratio is less than 0.5 we can conclude that these are soft magnetic particles[28]. The coercivity and the squareness ratio *R* are found to increase with increase in calcination temperature. These results confirm that as synthesized $BaWO_4$ nanoparticles are single domain particles[29]. As the calcination temperature increases the size of the particles increases. The coercivity of the single domain particle increases progressively with increase in particle size, because the magnetic moment of the individual particle increases. The magnetic moment of the individual particle increases with increase in particle size and hence, the retentivity of the particles increases. However, the exchange hardening of the soft magnetic particles begin to fail with further increase in particle size and hence the retentivity decreases[29].

4 Conclusions

$BaWO_4$ nanocrystalline samples are successfully prepared by direct chemical precipitation method without using any surfactant, templates or catalyst. From thermal studies, it is found that the synthesized $BaWO_4$ nanoparticles are thermally stable above 300 °C. The XRD spectral studies confirm tetrahedral structure for the synthesized $BaWO_4$ samples with a space group $I4_1/a$. The structural characterization confirms changes of particle size and surface morphology of $BaWO_4$ nanoparticles with increase in calcination temperature. The EDS study confirms the purity and elemental composition of the synthesized $BaWO_4$ sample. The optical bandgap energies of the $BaWO_4$ samples are also slightly changed with calcination treatment due to change in particle size caused by calcination. The PL spectra and CIE chromaticity diagram confirm the use of $BaWO_4$ nanocrystalline phosphors for fluorescent applications. From the VSM studies it is found that the synthesized $BaWO_4$ nanoparticles possess ferromagnetic behaviour at room temperature, and there is an anomalous variation of magnetic properties with calcinations temperature. Moreover, the synthesized $BaWO_4$ nanoparticle samples can be used in potential applications such as, optoelectronic devices and fluorescent and photocatalytic applications.

Acknowledgment

The authors acknowledge their thanks to Nanoscience Research Centre (NSRC), Nirmala College, Muvattupuzha for providing the opportunity to undertake this study. They are also thankful to SAIF, Cochin and SAIF Mahatma Gandhi University, Kottayam for providing facilities for characterization.

References

1 Sundaram R & Nagaraja K S, *Mater Res Bull*, 39 (2004) 581.
1 Edwin Suresh Raj A M, Mallika C, Sreedharan O M & Nagaraja K S, *Mater Lett*, 53 (2002) 316.
2 Lingna S, Minhua C, Yongheie W, Genban S & Changwen H, *J Crystal Growth*, 289 (2006) 231.
3 Karkkanen I, Kodu M, Avarmaa T, Kozlova J, Matisen L, Mandar H, Saar A, Sammelselg V & Jaaniso R, *Sci Direct Proc Eng*, 5 (2010) 160.
4 Jia G, Dong D, Song C & Zhang J, *Sci Adv Mater*, 6 (2014) 808.
5 Purnendu P, Karthik T N & Manivannan V, *J Alloys Compd*, 465 (2008) 380.
6 Shen Y, Li W & Li T, *Mater Lett*, 65 (2011) 2956.
7 Wang X, Xu H, Wang H & Yan H, *J Crystal Growth*, 284 (2005) 254.
8 Cavalcante L S, Sczancoski J C, Lima Jr L F, Espinosa J W M, Pizani P S, Varela J A & Longo E, *Crystal Growth Design*, 9 (2009) 1002.
9 Zawawi S M, Yahya R, Hassan A, Ekramul Mahmud H N M & Daud M N, *Chem Cent J*, 7 (2013) 118.
10 Vidya S, Solaman S & Thomas J K, *Adv Condensed Matter Phys*, 2013 (2013) 1.
11 Zawawi S M M, Yahya R, Hassan A & Daud M N, *Mater Res Innov*, 15 (2011) 97.
12 Zuwei S, Junfeng M, Xuyum L, Yong S, Jinrui F, Zhengsen L & Chang G, *J Am Ceram Soc*, 92 (2009) 1353.
13 Shi H, Wang X, Zhao N, Qi L & Ma J, *J Phys Chem B*, 110 (2006) 748.
14 Khademolhoseini S & Ali Z S, *J Mater Sci Matter Electron*, 27 (2016) 9605.

15 Cavalcantea L S, Sczancoski J C, Espinosa J W M, Varela J A, Pizani P S & Longo E, *J Alloys Compd*, 474 (2009) 195.
16 Lima R S, Anicete S M, Orhan E, Maurera M A, Souza A G, Pizani P S, Leite E R, Varela J A & Longo E, *J Luminescence*, 126 (2007) 741.
17 Mohamed Jaffer S M & Samson N A, *J Nanostruct Chem*, 5 (2015) 45.
18 Suryanarayana C & Norton MG, *X-ray diffraction:A Practical Approach* (Plenum Press, New York), 1998.
19 Sheena P A, Priyanka K P, Aloysius S N, Boby S & Thomas V, *Nanosyst Phys Chem Maths*, 5 (2014) 441.
20 Varghese T & Balakrishna K M, *Nanotechnology: An introduction to synthesis, characterization and applications of nanomaterials*, (Atlantic Publishers and Distributors: New Delhi), 2010.
21 Cullity B D, *Elements of X-ray diffraction*, Addison-Wesley, Reading MA, (1967) 388.
22 Lowell S, Shields J E, Thomas M A & Thommes M, *Characterization of porous solids and powders: Surface area, pore size and density*, (Kluwer Academic Publishers: The Netherlands), 2004.
23 Anukorn P, Dong J H, Suk J H, Somchai T & Jae S L, *J Mater Chem*, 20 (2010) 1683.
24 Pacheco-Torgal F, Lourenco P, Labrincha J, Chindaprasirt P & Kumar S, *Eco-efficient masonry bricks and blocks*, (Woodhead Publishing: UK), 2015.
25 Wenming T, Liping L, Wanbiao H, Tingjiang Y, Xiangfeng G & Guangshe L, *J Phys Chem C*, 114 (2010) 15298.
26 Anghel J, Thurber A, Tenne D A, Hanna C B & Punnoose A, *J Appl Phys*, 107 (2010) 09E314.
27 Fischer R, Schrefl T, Kronmuller H & Fidler J, *J Magn Magn Mater*, 153 (1996) 35.RJR
28 Rowlands G, *J Phys D: Appl Phys*, 9 (1976) 1267.